Prototype Tracking Studies for Proton CT

Jason Feldt, Jason Heimann, Nate Blumenkrantz, Dominic Lucia, Hartmut F.-W. Sadrozinski, *Senior Member, IEEE*, Abe Seiden, William Sowerwine, David C. Williams, Vladimir Bashkirov, Reinhard Schulte, Mara Bruzzi, David Menichelli, Monica Scaringella, G.A. Pablo Cirrone, Giacomo Cuttone, Nunzio Randazzo, Valeria Sipala, Domenico Lo Presti

***Abstract*–As part of a program to investigate the feasibility of proton computed tomography, the most likely path (MLP) of protons inside an absorber was measured in a beam experiment using a silicon strip detector set-up with high position and angular resolution. The locations of 200 MeV protons were measured at three different absorber depth of PMMA (3.75, 6.25 and 12.5 cm) and binned in terms of the displacement and exit angle measured behind the absorber. The observed position distributions were compared to theoretical predictions showing that the location of the protons can be predicted with an accuracy of better than 0.5mm.**

I. Introduction

PROTON radiation therapy is one of the most precise forms of non-invasive image-guided cancer therapy. It is based on the well defined range of protons in material, with low entrance dose, a dose maximum ("Bragg peak") and a rapid distal dose fall-off, providing better sparing of healthy tissue and allowing higher tumor doses than conventional radiation therapy with photons. At present, the potentials of proton therapy cannot be fully exploited because the conversion of Hounsfield values, measured with x-ray computed tomography (CT), to relative electron density values is not always accurate [1]. The resulting uncertainties can lead to range errors from several millimeters up to more than 1 cm depending on the anatomical region treated. Additional uncertainties exist with respect to the target position relative to normal tissues in the treatment room that could be minimized by using proton CT for guiding the therapy. The long-term goal of our project is to develop the capability to use proton CT (pCT) instead of x-ray CT to minimize these uncertainties. We plan to test the hypothesis that a proton CT system based on single-particle tracking can provide electron density maps for proton treatment planning and dose verification that are more accurate and at least as dose-efficient as electron density maps obtained with kV x-ray CT. In particular, we hypothesize that the range uncertainty of protons in the brain can be minimized from the current value of 3-10 mm, to 1-3 mm.

Previous work reviewed in [2] and our own preliminary studies [3-9] indicate that proton CT based on tracking of individual protons traversing an object from many different directions and measuring their energy loss and scattering angle may yield accurate reconstructions of electron density maps with good density and spatial resolution, despite the fundamental limitation of multiple Coulomb scattering (MCS).

TABLE I
COMPARISON BETWEEN X-RAY CT AND PROTON CT

	X-ray CT	**Proton CT**	**pCT Challenge**
Measurement Principle	X-ray Absorption	Proton Energy Loss	Good Energy Resolution
Ensemble	Statistical	Individual Protons	High Speed DAQ
Trajectories	Straight line	Curved due to Multiple Coulomb Scattering (MCS)	High Resolution Tracking Find MLP
Reconstruction	Filtered Back Projection	Layer-by-Layer de-convolution	Curved Trajectories

II. pCT: Measurement Principle and Limitations

The requirement to measure single protons leads to the following conceptual design of the pCT scanner [8]: the proton locations and directions at the entrance and exit of the phantom/patient are measured each with a telescopes consisting of two x-y planes of silicon detectors. The energy is measured in a hodoscopic array of calorimeter crystals. Details are given in Ref. [8].

The challenge of proton-by-proton pCT can be evaluate by a comparison with its established alternative, x-ray CT. This is shown in Table I. We have encouraging results in essentially all critical challenges shown in Table I. While x-ray CT uses a statistical evaluation of the absorption via the Photoelectric and Compton effects, pCT measures the energy loss of individual protons. In previous studies we showed high

Manuscript received November 9, 2005. This work was supported in part by the INFN 5th commission MOPI project.

J. Feldt, J. Heimann, N. Blumenkrantz, D. Lucia, H. F.-W. Sadrozinski, A. Seiden, W. Sowerwine and D. C. Williams are with SCIPP, UC Santa Cruz, CA 95064 USA (telephone: 831-459-4670, e-mail: hartmut @scipp.ucsc.edu).

V. Bashkirov and R. Schulte, are with Loma Linda University Medical Center, CA 92354 USA (e-mail: rschulte@dominion.llumc.edu).

M. Bruzzi, D. Menichelli, M. M.Scaringella are with INFN and Università di Firenze, Dipartimento di Energetica, Via S. Marta 3, 50139 Firenze, Italy, (telephone: +390554796350, e-mail: bruzzim @fi.infn.it).

G.A. P. Cirrone, G. Cuttone are with INFN Laboratori Nazionali del Sud, Via S. Sofia, Catania Italy (e-mail: cirrone@lns.infn.it).

N. Randazzo, V. Sipala, D. Lo Presti are with INFN Sezione di Catania, 64, Via S. Sofia, I-95123 Catania, Italy . V. Sipala and D. Lo Presti are also with Department of Physics, University of Catania, 64, Via S. Sofia, I-95123 Catania, Italy (e-mail: nunzio.randazzo@ct.infn.it).

contrast imaging using 140 MeV protons [3]. The dose is proportional to the square of energy resolution, thus mandating good energy determination. In addition to the energy resolution of the calorimeter, the energy resolution is limited by the natural energy straggling, which in 20 cm water is about 1-2%. Thus good energy resolution of better than 1% in the energy range from 100 to 200 MeV is required, and our results indicate that it can be achieved with crystals like CsI [9]. A detection of individual protons requires a data acquisition system capable of recording particle rates in excess of 1 MHz. We have developed such a system for the readout of silicon strip detectors [10]. The curved trajectories of the protons inside the phantom create difficulties for the image reconstruction as well, and instead of a straightforward filtered back projection (FBP) algorithm, a layer-by-layer de-convolution has been employed [11], [12].

In contrast to x-rays, which either transverse the phantom unchanged or are absorbed, allowing the reconstruction algorithm to deal with straight lines between the source and the detector, protons are undergoing MCS, which changes the direction depending on the amount of material traversed and the energy. This behavior is well understood [13] and allows reconstructing the most likely path (MLP) inside the absorber when the entrance and exit trajectories are measured external to the absorber. The exact behavior of the MLP as a function of material, depth, and displacement and scattering angle has been theoretically derived in [6] but needs to be verified experimentally.

Thus all challenges in the last column of Table I have been met with the exception of the experimental verification of the theoretical MLP prediction in the absorber (phantom, patient), the object of our beam experiment, described in detail below.

III. Most Likely Path

The theoretical MLP prediction and associated one sigma and 2-sigma envelopes [6] uses the well established Gaussian approximation of multiple scattering theory [13]. Fig. 1 shows predicted trajectories, indicating that the MLP depends strongly both on displacement and exit angle [6]. One can see that for typical MLPs the expected uncertainty is of the order of 300 μm. The objective of the tracking studies presented here was to verify the theoretical predictions by tracking individual protons inside a segmented absorber.

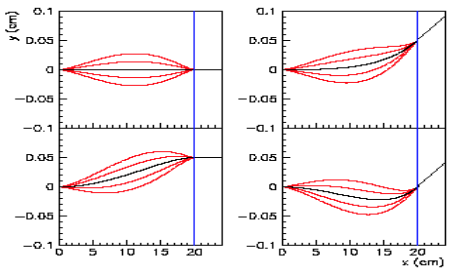

Fig. 1. Representative examples of MLPs including one- and 2-sigma envelopes of 200 MeV protons inside 20 cm of water [6].

IV. Beam Experiment Results: Tracking the Most Likely Path

A beam experiment with 200MeV protons was performed at the Loma Linda University Medical Center (LLUMC) synchrotron. The protons of 200 MeV energy were tracked with silicon strip detectors used before in the 1997 GLAST beam test [14]. In addition, a CsI calorimeter crystal provided energy measurement and a trigger for readout of the Si detector system.

A. Experimental set-up

The set-up consisted of x-y silicon modules used as entrance and exit telescope, and a CsI calorimeter (Fig. 2). The distance between the Si planes and the calorimeter was fixed during the runs. The set-up was flexible in that it allowed for insertion of 10 absorber plates (1.25 cm PMMA each) and a roving module between the telescopes. The following basic configurations were used: a) beam diagnostics, with two x-y planes both in entrance and exit telescopes, no absorber, b) MLP determination, with one entrance x-y plane and a roving plane between entrance and two exit Si planes. In the latter configuration, data were taken both without absorber (to check the alignment), and with absorber to map out the MLP at different depths within the PMMA stack with the roving module.

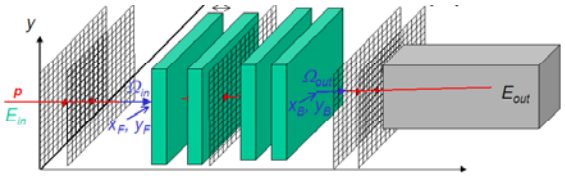

Fig. 2. Experimental layout: the 200MeV proton beam enters from left, is analyzed in the entrance telescope, passes through the segmented absorber (12 pieces of PMMA of 1.25 cm thickness each, and is again analyzed in the exit telescope before being stopped in the crystal. For beam diagnostic tests, the PMMA is removed and for MLP determination one of the entrance telescope planes is employed as a roving module.

For runs with absorber in place, the first entrance module was removed and inserted at various depths within the PMMA stack to act as the roving module. The three different locations of the roving module at 3.75 cm, 6.25 cm and 12.5 cm depth of PMMA, are shown in Fig. 3. The beam diagnostic configuration allowed measuring the entrance location and angle of the protons, i.e. the beam size and beam spread, while the MLP determination set-up measured only the entrance location and not the entrance angle of the proton. Since the MCS angle turned out to be much larger than the beam spread, this was an acceptable solution.

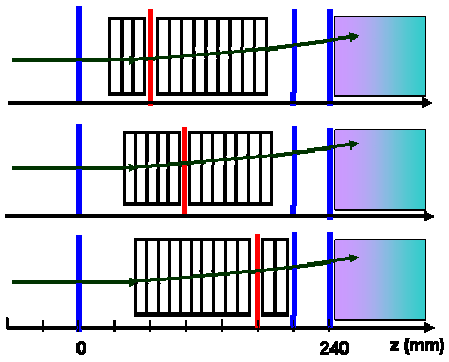

Fig. 3. Sketch of the three locations of the roving silicon module within the absorber stack (3.75 cm, 6.25 cm and 12.5 cm of PMMA, corresponding to z coordinates 6, 9 and 15cm).

B. Beam Characteristics

We measured the characteristics of the 200 MeV proton beam and found a correlation between angle and position in both the horizontal and vertical directions, indicating a focus at about 5 m upstream. The beam divergence was of the order of 5 mrad. This beam spread is much smaller than the expected MCS angle of about 50 mrad, within the stack of PMMA plates, so that there was no need to measure the entrance angle for mapping out the MLP. Instead, a dispersion correction based on the measured entrance position was applied in lieu of the entrance angle measurement. Since the silicon strips provided a position resolution of the order of 80 μm and therefore a good angular resolution (of the order of 0.003 rad) we expect that the beam divergence is the practical limit of our experimental resolution.

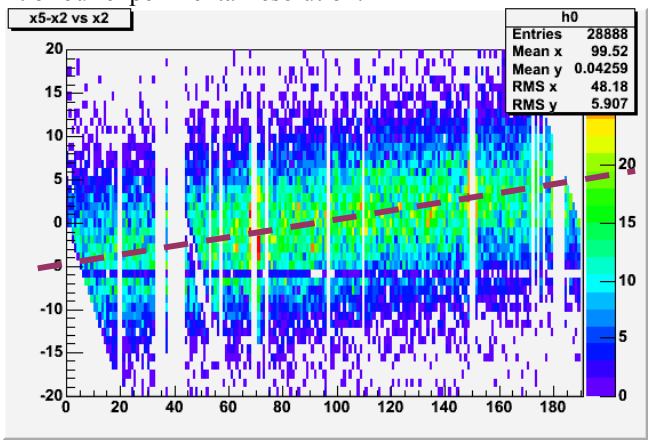

Fig. 4. Horizontal entrance angle vs. horizontal entrance position of the protons, both measured in number of strips. The beam spread is about 5 strips, corresponding to about 5 mrad. There is a clear dispersion, which can be explained with a "fuzzy" focal plane at an upstream distance of about 5 m.

C. Test of Multiple Coulomb Scattering Characteristics

The coordinates of the individual protons were transformed such that their entrance position and (inferred) direction was along the z-axis. Thus the x-y locations in the roving module and the exit telescope were expressed as the displacements relative to the initial proton direction, against which the exit angle was measured. The spread of the displacements at the three different locations of the roving module Y^{RMS}_{MCS} depends on the amount of absorber traversed and can be predicted by the Gaussian approximation of the MCS theory [13] . In addition the spread in the initial beam direction mentioned above caused an additional spread in displacements, Y^{RMS}_{beam}, which was determined by taking data without absorber. We expect that the observed Y^{RMS}_{ob} is the square root of the quadratic sum of these two contributions. In Table II we show the spread in the displacements as a function of the absorber depth. We find good agreement within 10-20%, indicating that the experimental spread is sufficiently explained by the beam characteristics and MCS. Thus, the intrinsic resolution of the instrument did not contribute significantly to the spread.

TABLE II
MEASURED AND PREDICTED SPREAD OF THE LATERAL DISPLACEMENTS IN THE ROVING MODULES AT DIFFERENT ABSORBER DEPTHS

Roving Location [cm]	No absorber Y^{RMS}_{Beam} [cm]	Absorb. (PMMA) depth [cm]	MCS Y^{RMS}_{MCS} [cm]	Expectation $\sqrt{(Y^{RMS}_{MCS})^2+(Y^{RMS}_{Beam})^2}$ [cm]	Data Y^{RMS}_{ob} [cm]
6	0.032	3.75	0.0334	0.046	0.055
9	0.046	6.25	0.0693	0.083	0.092
15	0.076	12.5	0.223	0.235	0.219

D. Most likely path as a function of the exit displacement and angle

With the absorber present, the exit displacement with respect to the entrance position and the exit angle were highly correlated because individual scattering events contribute both to the exit angle and the lateral displacement. The MLP analysis then correlates the position in the roving module (relative to the entrance position) with the exit displacement and angle. From Fig. 1 one expects a positive correlation between the lateral displacement in the roving module and the displacement, and a negative correlation between the position in the roving module and the exit angle.

The positions in the roving module are determined for bins in the displacement, where 5 strip width (~ 1.2 mm) is a realistic lower limit due to the beam spread mentioned before. This is shown in Fig. 5, where the position in the roving module at 7.5 cm depth is shown as a function of exit displacement, and as a function of exit angle for displacements between 2 and 4 mm. The expected correlations are indeed observed. The comparison between the measured displacements in the roving modules located at different depths within the absorber and the prediction of the MLP is shown in Fig. 6 for a few selected exit displacements. The data is binned in bins of 2 strips (= 472 μm) in exit displacement and averaged over all exit angles. The MLP prediction is then calculated for the means in displacement and angle.

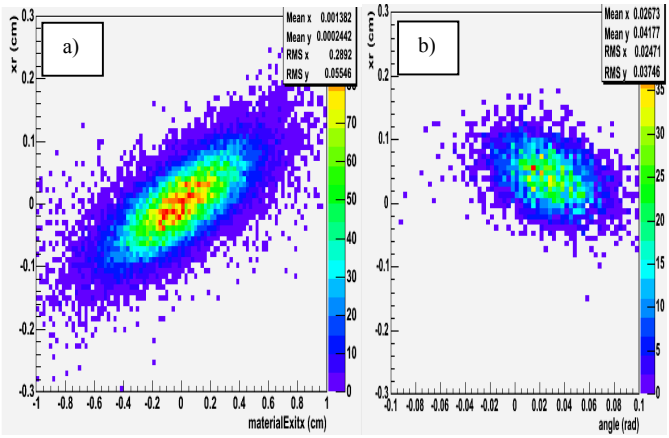

Fig. 5. Correlation between the displacement observed in the roving plane (vertical scale in cm) and exit parameters: on the horizontal scale: a) the displacement at the end of the absorber (in cm) and b) the exit angle (in rad) for the displacements between 0.2 and 0.4 cm.

This can only be a first step and has to be followed up by a procedure where the MLP is calculated for every proton and then averaged over, and a Monte Carlo study, including all instrument and beam effects. The experimental data are shown with their RMS variations.

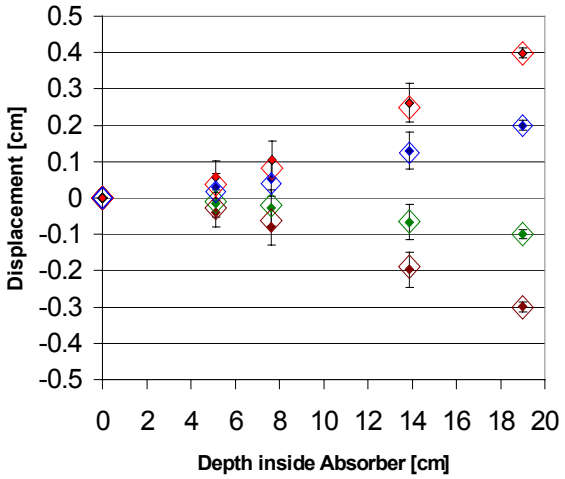

Fig. 6. Comparison of the displacement measured at the entrance, in the roving plane at different absorber depths and the absorber exit for 4 different exit displacements with the analytical calculation of the most likely path MLP (open symbols: the size of the symbol is close to the MLP spread). The absorber depth includes the ~1.5 cm free space in front of the roving plane. The external parameters used are: exit displacement bins of 500 μm and all angles accepted. At 7.5 cm depth, the MLP predicts a one sigma band of 380 μm, while the measurement has an RMS = 490 μm, due to the beam finite spread.

It is encouraging that at this level, the prediction of the MLP is verified by the data within less than 200 μm, much less than the experimental spreads. Moreover, the apparent increasing systematic disagreement between the experimental means and the MLP predictions for larger exit displacements can be explained by the fact that the roving modules are preceded and followed by a ~1.5 cm long space without absorber, which is not described in the MLP prediction and causes the MLP prediction to be underestimated by up to 200 μm,

E. Spreads in the Displacement Distributions within the Absorber

There are three different effects that can influence the spread in the roving modules. As mentioned before, the finite beam spread influences the spread of the experimental distributions. This has to be simulated with a full Monte Carlo program. Another is the bin size of the exit displacement selected. The third is introduced when defining the exit angle.

TABLE III
MEASURED SPREAD IN THE ROVING MODULES IN CM AS A FUNCTION OF EXIT BIN WIDTH IN NUM BER OF STRIPS

z [cm]	Bin Width (number of strips)					
	20	10	5	2	1	MLP
6	0.042	0.041	0.042	0.044	0.038	0.027
9	0.061	0.056	0.055	0.051	0.051	0.038
15	0.094	0.068	0.058	0.054	0.055	0.031

Both the experimental spreads and the expected MLP spread are constant at a constant roving location for all displacements at the absorber exit. The spreads in the roving modules as a function of exit displacement bin size are shown in Table III. For comparison, the spreads of the MLP are shown. The results indicate that for the present data where the input angle is not measured and the data are averaged over the beam spread, the spreads do not improve at smaller exit displacement bin widths than about 5 strips (= 1.18mm), as expected from the observed beam spread.

A marked reduction of the spread of the displacement in the roving module was observed when the information provided by the exit angle was used. Fig. 7 shows the measured mean displacement in the roving module at different absorber depths for an exit displacement of 2 mm, for three small bins of exit angles at the mean and the mean ± 1 angle sigma. The selected exit angles are within ± 0.0036 rad of the selected means. The means of the displacements in the roving modules separate on the level of 100 – 200 μm. The achieved spreads in displacements within the absorber as a function of the angular selection are shown in Table IV. The spreads are independent of the exit displacement selected, and show a remarkable improvement when the angle is selected.

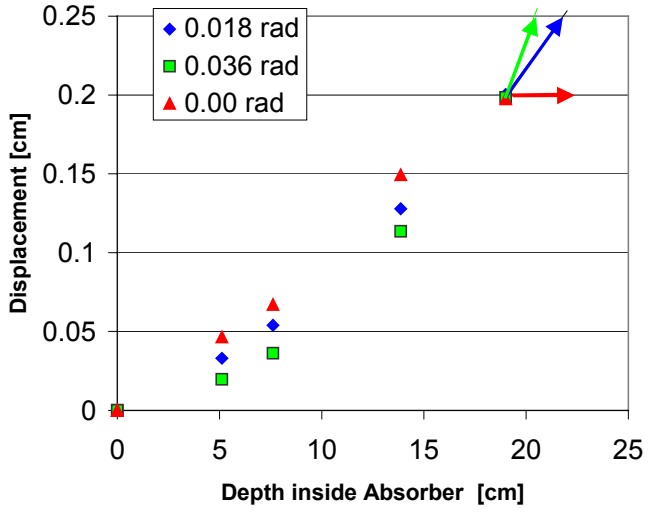

Fig. 7. Measured displacement in the roving modules at three different absorber depth for an exit displacement of 2 mm, for three different exit angle bins of equal bin size of ±0.0036 rad centered at an exit angle of 0.018 (mean of all angles), 0.036 (+ 1 exit angle σ) and 0.000 (-1 exit angle σ)). The absorber depth include the ~1.5 cm free space in front of the roving module.

TABLE IV
MEASURED SPREAD (CM) IN THE ROVING MODULES AS A FUNCTION OF ANGLE SELECTION

	Selection on Angles				
z [cm]	All	0.033 rad	0.066 rad	0.0 rad	MLP
6	0.038	0.033	0.029	0.034	0.027
9	0.049	0.043	0.041	0.041	0.038
15	0.054	0.039	0.035	0.038	0.031

The beam test proves that already at this stage, the location of the proton within the phantom/patient can be predicted to better than 0.5 mm, validating the MLP approach which uses only **external** track information for the prediction of the trajectories **inside** the phantom/patient. More Monte Carlo simulations are under way [15].

V. FUTURE PLANS

The next steps are a beam test with an in-homogenous absorber (i.e. holes and inclusions at certain depths), followed by CT studies using a rotating phantom. This will require the use of both the tracker (measuring both positions and angles at both entrance and exit) and the calorimeter, exploiting the full power of the pCT scanner.

VI. CONCLUSIONS

We have measured the most likely path of 200 MeV protons inside a segmented absorber of PMMA. The displacements of the protons from their original path agree well with the theory of multiple Coulomb scattering (MCS). We show that as expected from the theory of the most likely path (MLP) [6], we can predict the trajectory of the proton inside the absorber to better than 0.5 mm. This number is expected to improve when the effect of the beam divergence is eliminated with a measurement of the entrance angle of the proton.

ACKNOWLEDGMENT

We appreciate the smooth running of the LLUMC synchrotron. This work was supported by Calspace and MOPI project, INFN 5th commission.

REFERENCES

[1] B. Schaffner and E. Pedroni, "The precision of proton range calculations in proton radiotherapy treatment planning: experimental verification of the relation between CT-HU and proton stopping power", *Phys Med Biol*. 43(6):1579-1592, 1998.

[2] H. F.-W. Sadrozinski, V. Bashkirov, B. Keeney, L. R. Johnson, S. G. Peggs, G. Ross, T. Satogata, R. W. M. Schulte, A. Seiden, K. Shanazi, and D. C. Williams, "Toward proton computed tomography", *IEEE Trans. Nucl. Sci*, vol 51, no.1, pp. 3-10, Feb. 2004.

[3] L. R. Johnson, B. Keeney, G. Ross, H. F.-W. Sadrozinski, V. Bashkirov, R. W. Schulte, K. Shahnazi. "Initial studies on proton computed tomography using a silicon strip detector telescope", *Nucl Instr Meth* **A** 514 (2003) 215.

[4] HF-W Sadrozinski, M. Bruzzi, L.R. Johnson, B. Keeney, G. Ross, A. Seiden, D. C. Williams, L. Zhang, V. Bashkirov, R. W. Schulte, K. Shahnazi. "Issues in proton computed tomography", *Nucl Instr Meth* **A** 511: (2003) 275-281.

[5] L. R. Johnson, B. Keeney, G. Ross, H. F.-W. Sadrozinski, A. Seiden, D. C. Williams, L. Zhang,V. Bashkirov, R. W. Schulte, K. Shahnazi, "Monte Carlo studies on proton computed tomography using a silicon strip detector telescope". SCIPP 02/35.

[6] D C Williams, "The most likely path of an energetic charged particle through a uniform medium", *Phys. Med. Biol*. 49 2899-2911, 2004.

[7] R. W. Schulte, V. Bashkirov, M. C. Klock, T. Li, A. J. Wroe, I. Evseev, D. C. Williams, T. Satogata, "Density resolution of proton computed tomography", *Med Phys. 2005, 32:1035-46*

[8] R. W. Schulte, V. Bashkirov, B. Keeney, L. R. Johnson, H. F.-W. Sadrozinski, A. Seiden, D. C. Williams, L. Zhang, "Conceptual design of a proton computed tomography system for applications in proton radiation therapy", *IEEE Trans. Nucl. Sci., vol 51, no.3, pp 866 – 875, June 2004.*

[9] M. C. Klock, R. W. Schulte, V.Bashkirov, "First experimental calorimeter studies for proton CT at LLUMC", *unpublished.*

[10] H. F.-W. Sadrozinski, V. Bashkirov, M. Bruzzi, M. Ebrahimi, J. Feldt, J. Heimann, B. Keeney, F. Martinez-McKinney, D. Menichelli, G.Nelson, G. Nesom, R. W. M. Schulte, A. Seiden, E. Spencer, J. Wray, and L. Zhang, "The particle tracking silicon microscope PTSM", *IEEE Trans. Nucl. Sci., vol* 51, no.5, pp 2032 – 2037, Oct 2004.

[11] T. Li, Z. Liang, et al. " Reconstruction with most likely trajectory for proton computed tomography", *SPIE Medical Imaging*, 2004.

[12] T Li, Z. Liang, K. Mueller, J. Heimann, L. Johnson, H. F.-W. Sadrozinski, A. Seiden, D. Williams, L. Zhang, S. Peggs, T. Satogata, V. Bashkirov, and R. W. Schulte, "Reconstruction for proton computed tomography: a Monte Carlo study", *IEEE NSS/MIC Conf Record* 2003

[13] Particle Data Group, S. Eidelman et al., "Review of Particle Physics", *Physics Letters* B 592, 1 (2004).

[14] W. B. Atwood, S. Ritz, P.Anthony, R.P.Johnson, W.Kroeger, H.F.-W.Sadrozinski et *al.,* "Beam test of Gamma-ray Large Area Space Telescope components", *Nucl.Instrum.Meth*. A446 (2000) 444-460.

[15] G. A. P. Cirrone et *al*, "Detailed Monte Carlo Investigation of a Proton Computed Tomography System", Poster J03-25, 2005 IEEE NSS-MIC Symposium in Puerto Rico, Oct 2005.